Interstitial pH and pO_2 gradients in solid tumors *in vivo*: High-resolution measurements reveal a lack of correlation

GABRIEL HELMLINGER, FAN YUAN, MARC DELLIAN & RAKESH K. JAIN

Edwin L. Steele Laboratory, Department of Radiation Oncology, Massachusetts General Hospital, Harvard Medical School, Boston, Massachusetts 02114, USA

The partial pressure of oxygen (pO_2) and pH play critical roles in tumor biology and therapy. We report here the first combined, high-resolution (≤10 μm) measurements of interstitial pH and pO_2 profiles between adjacent vessels in a human tumor xenograft, using fluorescence ratio imaging and phosphorescence quenching microscopy. We found (1) heterogeneity in shapes of pH and pO_2 profiles; (2) a discordant relation between *local* pH profiles and corresponding pO_2 profiles, yet a strong correlation between *mean* pH and pO_2 profiles; (3) no correlation between perivascular pH/pO_2 and nearest vessel blood flow; and (4) well-perfused tumor vessels that were hypoxic and, consequently, large hypoxic areas in the surrounding interstitium. Such multiparameter measurements of the *in vivo* microenvironment provide unique insights into biological processes in tumors and their response to treatment.

Oxygen and pH are key microenvironmental factors in the development and growth of tumors and their response to treatment. Oxygen and pH levels affect tumor cell metabolism, glucose and oxygen consumption rates, and tumor cell proliferation and viability[1–4]. Hypoxia can stimulate angiogenesis[5]. Hypoxia can also induce tumor cell apoptosis[6], as well as select for cells with defects in apoptosis[7], thereby affecting tumor growth. Tumor cell migration and immune cell response are other key processes in tumor biology that may be influenced by the levels of pH and oxygen in the extracellular milieu[8–11].

The partial pressure of oxygen (pO_2) and pH also play important roles in the response of tumors to radiation, chemotherapy, hyperthermia and photodynamic therapy[12–16]. The selective microenvironmental characteristics displayed by tumors, such as interstitial acidity and hypoxia[1,13–15,17,18] may be either propitious or unfavorable for cancer treatment depending on the type of therapy considered. The situation is further complicated because of marked intra- and inter-tumor variations in interstitial pH and pO_2. Hypoxic tumor cells have long been known to be radiation resistant[19]. During chemotherapy, hypoxia may either enhance cell kill, as in the case of bioreductive drugs[20] and alkylating agents[21], or reduce cell kill, as in the case of bleomycin or actinomycin D (ref. 22). Similarly, acidic pH potentiates the cytotoxicity of alkylating drugs[1,23] and weak acids[4,25], decreases the efficacy of other anticancer drugs (for example, adriamycin, bleomycin), and may affect radiation sensitivity[13]. Consequently, tumor pH and pO_2, as well as related metabolic parameters such as lactate level, have been proposed as prognostic factors in various cancer therapies[26,27] and metastases[28,29].

Clearly, a high-resolution, dynamic mapping of spatial and temporal pH/pO_2 profiles in tumors *in vivo* is needed for a quantitative assessment of the role of pH/pO_2 in tumor progression and response to therapies. Techniques such as electrode measurements[30], nuclear magnetic resonance[31], positron emission tomography[32], biomarker measurements[3] and implantable microchambers[34] either do not provide sufficient temporal or spatial resolution, are invasive, or cannot be combined for simultaneous measurements.

Here we present combined fluorescence ratio imaging microscopy (FRIM) and phosphorescence quenching microscopy (PQM) techniques to quantify, simultaneously, pH and pO_2 profiles *in vivo*. Unique aspects of our approach include high spatial resolution (5 × 5 μm for pH, 10 × 10 μm for pO_2), repeated measurement capability (for example, before and after treatment of a tumor), noninvasiveness, correlation with local hemodynamic parameters and applicability to thick (>1 mm) tissues. We demonstrate (1) a spectrum of shapes of interstitial pH and pO_2 profiles in a human tumor xenograft; (2) a discordant relation between *local* pH profiles and corresponding pO_2 profiles, yet a strong correlation between *mean* pH and pO_2 profiles, with pronounced gradients when measurements are taken moving away from the nearest blood vessel; and (3) no correlation between perivascular pH/pO_2 and local blood flow.

Spatial heterogeneity in pH and pO_2 profiles

High-resolution FRIM and PQM techniques were implemented as shown in Fig. 1 (see the Methods section). Tumor locations and corresponding pH/pO_2 profiles were recorded in LS174T human colon adenocarcinoma xenografts (Fig. 2). The majority (>90%) of intervessel pH profiles exhibited pronounced gradients, with highest pH proximal to blood vessels and lowest pH distant from vessels (Fig. 2, *b, d, f* and *h*). However, intervessel pH gradients occasionally exhibited sections with a flat profile in avascular areas (Fig. 2*h*). Areas with no pronounced intervessel pH gradient were also detected (Fig. 2*j*). Corresponding intervessel pO_2 profiles exhibited a variety of shapes; some were flat (Fig. 2*b*), some had parabolic-like shapes as reported above for pH gradients, and some exhibited monotonic profiles from one vessel to another (Fig. 2, *d, f* and *j*). Between two vessels, the shapes of the pH and corresponding pO_2 profiles did not necessarily match (Fig. 2, *b, d, f* and *h*). Large, well-perfused tumor vessels (≥20-μm diameter) with hypoxic pO_2 values (≤5 mmHg) were also detected (Fig. 2, *f* and *j*). In some tumors, large avascular areas developed (≥1 mm; Fig. 2*g*). In such areas, interstitial pH dropped to unusually acidic values (range: 6.6–6.8) and pO_2 to extremely

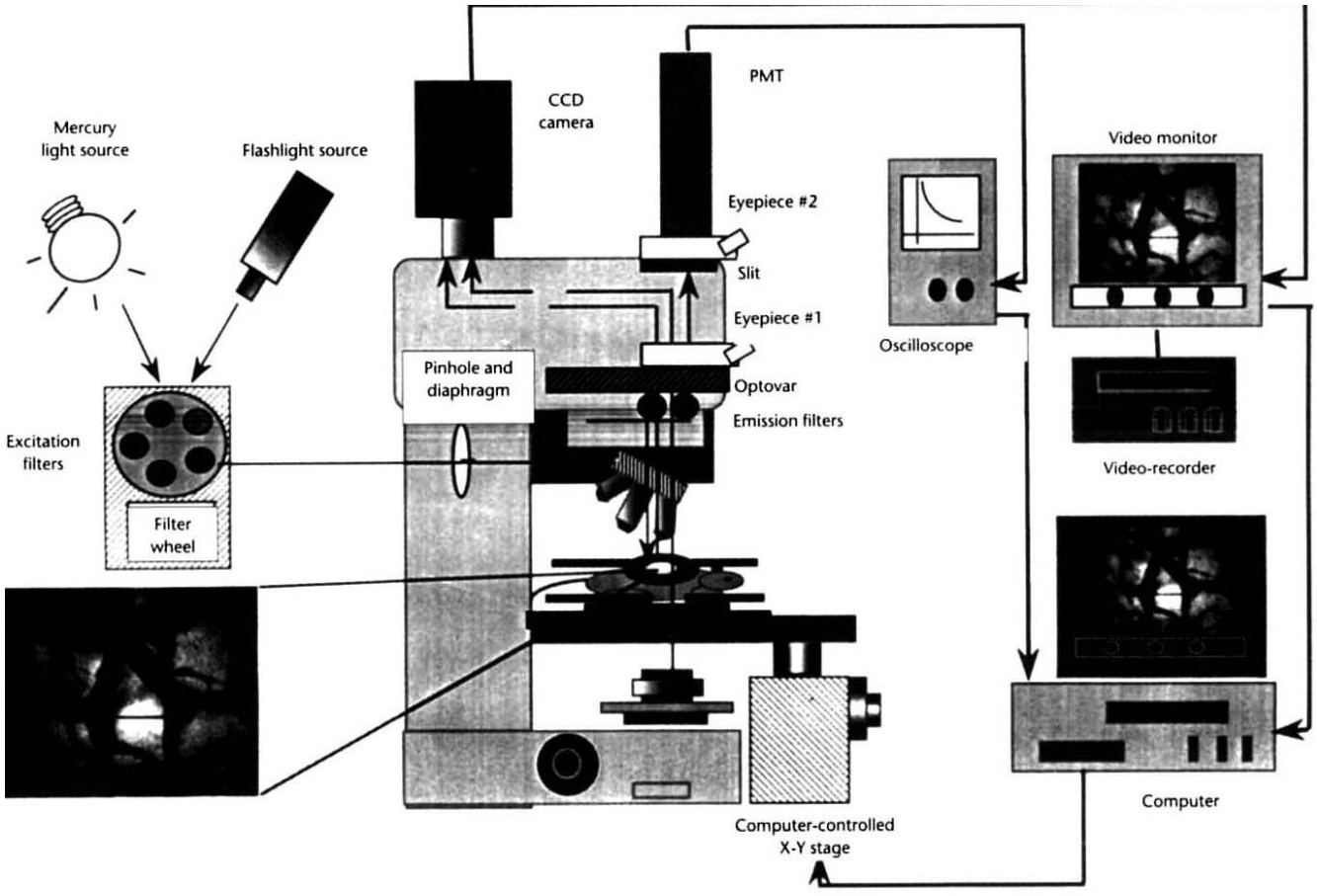

Fig. 1 Experimental station for combined measurements of pH and pO_2 profiles in a human tumor xenograft model, using fluorescence ratio imaging (pH) and phosphorescence quenching (pO_2).

hypoxic values (≤0.5 mmHg) (Fig. 2*h*). A study of the time dependence of pH and pO_2 showed that pH profiles were very stable within a 1-hour period (≤0.02 pH unit variation). pO_2 profiles, however, could vary by ±3 mmHg within the same time frame (data not shown).

Mean pH and pO_2 profiles

We next obtained mean interstitial pH and pO_2 profiles when measurements were taken moving distally from the nearest blood vessel, by averaging single-scan profiles. For an intervessel distance of *D*, interstitial profiles were averaged over a distance of *D/3*, so that the influence of the second nearest vessel on pH and pO_2 would be negligible. The mean pO_2 profile decreased monotonically (Fig. 3), and hypoxic values (≤5 mmHg) were reached 70–80 µm away from the nearest vessel wall. Near anoxic values (0.0–0.5 mmHg) were consistently found ≥150 µm away from the vessel wall. The transvascular pO_2 gradient [defined as $\Delta pO_2 = pO_2$ (center of vessel) – pO_2 (50 µm from vessel wall)] was more pronounced in tumor tissue ($\Delta pO_2 = 5.5$ mmHg), where the vasculature was heterogeneous, as compared with that of normal subcutaneous tissue ($\Delta pO_2 = 1.9$ mmHg), where the capillaries underlying the larger vessels in the plane of focus were spatially uniform (Fig. 3, inset).

In tumors, the mean pH profile also decreased, with a mean pH drop of 0.32 between 10 and 100 µm away from the vessel wall (Fig. 3). It is particularly interesting that the mean pH profile exhibited a plateau phase (pH ≈ 6.91) between 100 and 170 µm, while pO_2 kept decreasing. In anoxic regions (≥170 µm), pH decreased further ($P < 0.01$) to reach a second plateau phase (pH ≈ 6.70 at ≥270 µm; ΔpH = pH at 170 µm – pH at 270 µm = 0.21; Fig. 3). Standard errors were larger for pO_2, as compared with pH (Fig. 3), because of a more pronounced heterogeneity in pO_2 profiles (Fig. 2). A strong correlation was found (Spearman correlation: $r_s = 0.980$; linear curve fit: $r = 0.931$) between the mean pH and mean pO_2 values reported in Fig. 3.

Relation between pH and pO_2

A scattergram of combined pH/pO_2 measurements at randomly selected interstitial locations (without reference to the vessel distance) is depicted in Fig. 4. In 27-day-old tumors, no correlation between pO_2 and pH was found ($r_s = 0.443$). Interstitial pO_2 values ranged from 0 to 25 mmHg for pH ≥7.0. it is noteworthy that hypoxic or anoxic pO_2 values were obtained in regions of relatively normal pH (≥7.2). Also, the majority of pO_2 measurements were hypoxic or anoxic when the pH dropped below a value of 7.0 (Fig. 4). The mean values of interstitial pH and pO_2 in 27-day-old tumors were 7.04 ± 0.02 (±s.e.m.; median: 7.07) and 8.3 ± 1.6 mmHg (median: 6.41), respectively (Fig. 5). In 17-day-old tumors, only a moderate correlation was found between pO_2 and pH ($r_s = 0.617$). In particular, pO_2 values ranged from 0 to 26 mmHg within a narrow pH range of 6.9–7.1. However, no hypoxic values were found at pH ≥7.1 (Fig. 4). In these tumors, the mean interstitial pH (7.04 ± 0.03; median: 7.02) was virtually equal to, but the mean pO_2 (15 ± 3.0; median: 15.0) was higher

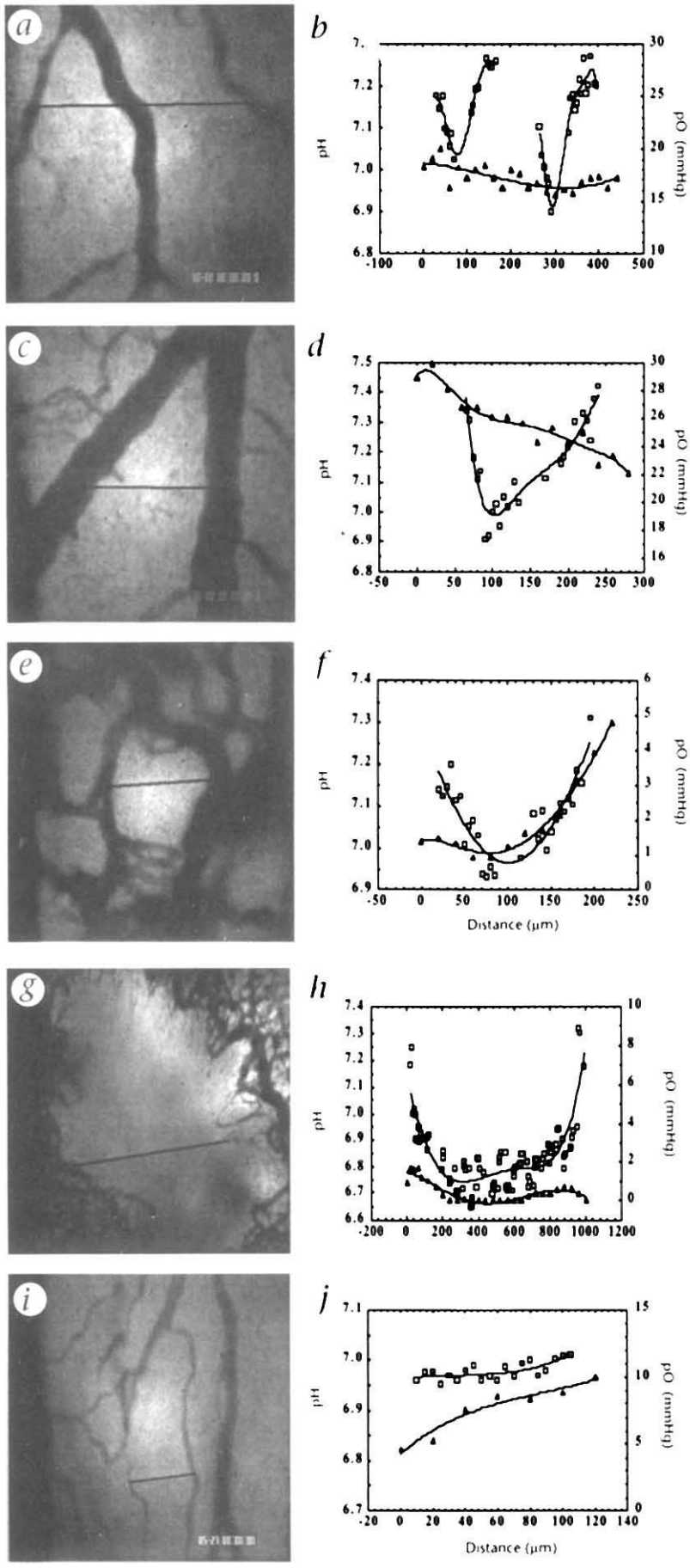

Fig. 2 Combined measurements of intervessel pH/pO_2 profiles. *left*, Transillumination image of tumors. *right*, Corresponding pH/pO_2 profiles. Black bar in tumor image indicates location where profiles were measured. First (0-μm abscissa) and last points correspond to the centers of the two vessels delimiting the interstitial measurements. Scale on *x*-axis (scale differs among subplots). Open symbols, pH; closed symbols, pO_2. *a–h*, Images and graphs from 27-day-old tumors; *i* and *j*, from 17-day-old tumors.

than ($P < 0.01$), the mean values found in older tumors (Fig. 5). Normal subcutaneous scattergram points and mean pH and pO_2 values are given as controls (Fig. 4 and 5); mean values were significantly higher ($P < 0.01$) as compared with those of tumor tissue.

Relation between blood flow and pH/pO_2

When the vessel was clearly in focus under transillumination, local blood flow was measured before and after the pH/pO_2 measurements. The variation of perivascular pH and pO_2 (combined measurements 50 μm away from the vessel wall) with blood flow rate of the nearest vessel, obtained after the pH/pO_2 measurements, is shown in Fig. 6. No correlation was found between either pH and flow rate ($r_s = 0.229$), or pO_2 and flow rate ($r_s = 0.422$). Also, there was no correlation between intravascular pO_2 and flow rate ($r_s = 0.467$; not shown). In particular, vessels with a high flow rate but hypoxic pO_2 values were detected. Similarly, neither pH nor pO_2 correlated with blood flow obtained before the pH/pO_2 measurements (not shown), although blood flow in a given vessel could change dramatically during the course of an experiment. Finally, neither pH nor pO_2 correlated with the two measured parameters used to compute flow rate, namely, red blood cell velocity (range: 0.077–0.805 mm/s) and vessel diameter (range: 10–80 μm) (not shown).

Discussion

Implication for therapy. This study demonstrates, for the first time, widely heterogeneous patterns of high-resolution pH and pO_2 profiles in a human tumor xenograft. Such patterns may be at least partially responsible for the low success rate observed during chemotherapy of common adult solid tumors. Apart from drug delivery issues[35], a given therapeutic agent operating within narrow pH and pO_2 ranges will not be equally effective in interstitial areas exhibiting steep gradients (Fig. 2). A similar argument could be made to explain limitations of radiation therapy. The situation is worsened considering that we found a disparate relation between pH and pO_2 *in vivo*; hypoxic regions (≤5 mmHg) were detected, concomitantly with a normal pH (≥7.2) (Figs. 2, *f* and *h*, and 4). This could exert antagonistic effects on the action of certain classes of chemotherapeutic drugs. Alkylating agents, for example, are most effective in hypoxic *and* acidic regions.

The present work has further implications for

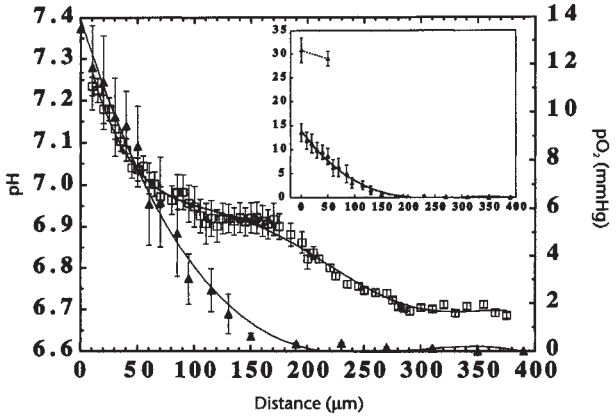

Fig. 3 Mean interstitial pH and pO_2 profiles of 27–day-old tumors taken as one moves away from the nearest blood vessel (± s.e.m., $n = 24$ profiles, $N = 7$ tumors). Open symbols, pH; closed symbols, pO_2. *inset*, pO_2 gradients in tumor (▲; same curve as in large plot) and normal tissue (△; $n = 15$, $N = 3$). For both plots, 0-μm abscissa corresponds to the center of the nearest vessel. Scale thereafter corresponds to distance from the vessel wall.

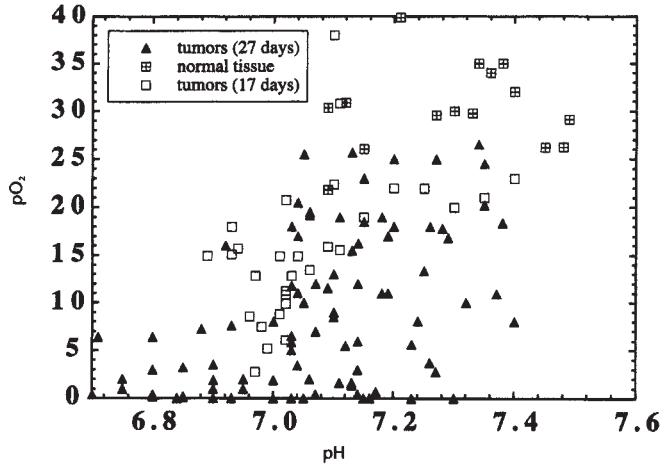

Fig. 4 pH/pO_2 scattergram at various interstitial locations. Spearman correlations and linear curve fits, respectively: $r_s = 0.44$, $r = 0.47$ (27-day-old tumors); $r_s = 0.62$, $r = 0.51$ (17-day-old tumors); $r_s = 0.03$, $r = 0.10$ (normal tissue).

therapies based on white blood cell-mediated cytotoxicity, which is known to be inhibited under certain pH and pO_2 conditions *in vitro*[11]. Indeed, a spectrum of immune cell and inflammatory cell responses is expected, considering (1) the wide distribution of perivascular pH and pO_2 values (Fig. 2); (2) a moderate or no correlation between local pH and pO_2 (Fig. 4); and (3) pronounced interstitial gradients (Fig. 2). Thus pH and pO_2 levels that inhibit immune/inflammatory responses may develop locally in tumors *in vivo*.

Interstitial pO_2 depends on blood flow, intravascular pO_2 and the metabolic consumption rate of the cells. In our experiments, blood flow in a given vessel could vary substantially during the course of an experiment. However, whether we considered blood flow before (not shown) or after (Fig. 6) the pH/pO_2 measurements, we found no correlation between local blood flow and either perivascular pH or pO_2. In particular, well-perfused tumor blood vessels were detected which were hypoxic (Fig. 2, *e* and *f*). This provides a basis for explaining the limited success of adjuvant therapies aimed at increasing tumor blood flow, in order to increase tumor oxygenation and/or drug delivery. Based on our results, increased oxygenation will not necessarily correlate uniformly with improved blood flow. Also, assuming a drug is present at higher concentrations owing to improved blood flow, it could still face a highly heterogeneous pH and pO_2 microenvironment and fail locally.

Implication for tumor metabolism. This study also provides important insights into tumor metabolism. Tumor cells are often viewed as high lactate and H^+ producers, because of intense glycolytic activity under hypoxic conditions[36]. In the present model, the mean interstitial pH profile exhibited a mean drop of 0.32 from 10 μm (pH = 7.24) to 100 μm (pH = 6.92) away from the vessel wall, with decreasing (from 14 to 3 mmHg) pO_2 conditions (Fig. 3). Such pH values and gradients are very similar to those observed in multicellular tumor spheroids *in vitro*. However, surface pO_2 is an order of magnitude higher (100–120 mmHg) and the subsequent pO_2 gradient into the spheroid is steeper[37,38]. Lower pO_2, therefore, is not necessarily correlated with lower pH *via* increased glycolysis. This is consistent with earlier findings in tumors *in vivo*, where no metabolic shift from

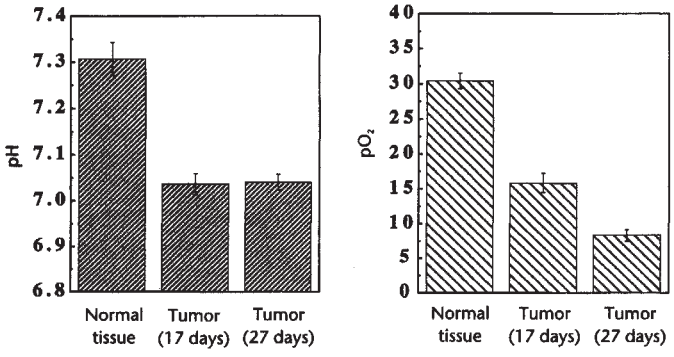

Fig. 5 Combined mean (±s.e.m.) pH and pO_2 of tumor and normal subcutaneous interstitial tissues. Data were computed from scattergram points of Fig. 4. For 27-day-old tumors: $n = 96$ points, $N = 8$ tumors; for 17-day-old tumors: $n = 31$, $N = 5$; normal tissue: $n = 15$, $N = 3$.

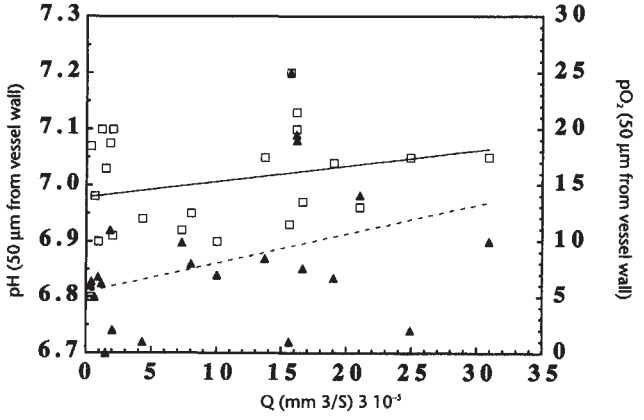

Fig. 6 Combined measurements of interstitial pH/pO_2 and blood flow rate of nearest vessel ($n = 23$ locations, $N = 6$ tumors). Open symbols, pH; closed symbols, pO_2. Spearman correlations and linear curve fits, respectively: $r_s = 0.23$, $r = 0.26$ for pH vs. Q; $r_s = 0.42$, $r = 0.51$ for pO_2 vs. Q for 27-day-old tumors.

respiration to glycolysis could be found when a deficient oxygen supply was imposed[2]. Further evidence supports this hypothesis: while pO_2 decreased to near anoxic values (between 100 and 170 μm), interstitial pH exhibited a plateau phase (Fig. 3); also, mean tumor pH remained stable while mean pO_2 decreased, when tumors became older (27 vs. 17 days, Fig. 5). Alternatively, the pH plateau phase (between 100 and 170 μm; Fig. 3) may reflect a lack of glucose availability at such interstitial distances[9], which would limit glycolysis and hence H^+ production. Metabolic rates may also differ among heterogeneous tumor cell populations. A further pH decrease was observed in anoxic regions (Fig. 3), and only low pH values (≤6.90) were recorded in extremely hypoxic regions (Fig. 4). Under such conditions, nutrient availability is presumably very limited, and both oxygen and glucose consumption rates are diminished[3]. However, excessive waste accumulation over time might contribute to further tissue acidification.

The combined, high-resolution profiles reported here are well within the range of previous separate measurements of tumor pH and pO_2 *in vivo*[30,40–43]. The combined use of the FRIM-PQM station with other *in vivo* or *in vitro* techniques will allow to address quantitative issues on oxygen and pH in tumor metabolism, angiogenesis, growth and regression, and cell migration. Also, FRIM of other ratiometric probes (for example, for Ca^{2+}, Na^+, membrane potential) *in vivo* may be developed to elucidate dynamic cell signaling events involved in tumor biology and response to treatment.

Methods

Experiments were performed on LS174T human colon adenocarcinoma grown in a transparent dorsal window chamber in mice with severe combined immunodeficiency disease (SCID mice)[4]. Chambers without tumor cells (normal subcutaneous tissue) served as controls. The awake animal was immobilized in a polycarbonate tube (25-mm inner diameter) on a motorized X-Y stage (±0.5-μm resolution; Burleigh Instruments, Fishers, NY), in the illumination field of a fluorescence microscope (Axioplan, Zeiss, Jena, Germany). The stage allowed the selection of tumor locations for "single-point" or intervessel profile (steps of 20.0 ± 0.5 μm) measurements (Fig. 1). Background and fluorescence images at all selected locations were first recorded for pH determination, followed by pO_2 measurements. Transillumination of local vessels was videotaped (1 min) at the start and end of the experiment for the off-line determination of blood flow[43].

pH measurements — Fluorescence ratio imaging microscopy (FRIM). The free acid, cell-impermeant form of the H^+-sensitive fluorochrome 2′,7′-bis-(2-carboxyethyl)-5,6-carboxyfluorescein (BCECF, Molecular Probes, Eugene, OR) was injected into the tail vein (0.7 mg/kg). After 15 min, fluorescence emission images (535-nm filter, Oriel, Stratford, CT) were recorded with a charge-coupled device (CCD) camera (C2400-88, Hamamatsu, Bridgewater, NJ) following 440-nm and 495-nm excitation (Oriel). The ratio image was formed as follows: $R_{535} = (I_{495} - I_{back495})/(I_{440} - I_{back440})$. Background images at each wavelength ($I_{back440}$, $I_{back495}$) were recorded before dye injection and subtracted from the corresponding fluorescence images (I_{440}, I_{495}). Probe fluorescence at 440 and 495 nm was typically 3 to 5 times higher than the corresponding background fluorescence.

To circumvent optical problems associated with quantitative microscopy of thick tissues, we devised a partial confocal effect by placing a 40-μm pinhole in the excitation light path (Fig. 1)[43]. *In vitro* tests were performed to determine the depth of light collection. A variable number of thin, flat aluminum foil sheets were placed between two glass coverslips, with a central channel of variable depth containing a thin film of a BCECF-fluid mixture of known pH. Color marks were left on the fluid-facing side of the two coverslips to allow for a precise measure of fluid depth *via* the calibrated microscope stage (±0.5 μm vertical resolution). The smallest depth (15 ± 2.0 μm) was obtained by placing a film of fluid between the two coverslips (no aluminum foil). A depth of light collection of 25 μm was determined while preserving an adequate signal-to-noise ratio, using a ×40 water immersion objective (NA 0.75, Achroplan, Zeiss). A lateral spatial resolution of 5 × 5 μm² was obtained.

Calibration experiments with capillary tubes *in vitro* as well as excised tissues (tumor and normal skin) showed that ratios of fluorescence intensity were linearly proportional ($r^2 \geq 0.98$) to pH in the physiological range of 6.20–7.80 (ref. 43). The FRIM technique was applicable only for interstitial pH measurements. It did not apply to vascular locations, as light absorption by blood hemoglobin differed for the two excitation wavelengths used[43]. Interstitial pH values were valid at a ≥10-μm distance from the nearest vessel wall, when the fluorescence illumination spot was beyond any vascular structure.

Because the sampling depth was 25 μm (see above), a systematic error was introduced when estimating a plane measurement from an actual three-dimensional, 25-μm-deep tissue slice. We estimated this error as follows: the actual data were fitted with a polynomial function $P(r)$, where r is the radial coordinate. The (r,Θ) coordinate system [where $(r,0)$ refers to the measurement axis] was replaced by (x,y,z) coordinates, with $r^2 = (x^2 + z^2)$ and z the vertical coordinate (depth of tissue). $P[(x^2 + z^2)^{1/2}]$ was integrated over a depth of $z = 25$ μm, and the resulting curve was compared with the original data fit $P(r)$. The maximal error at any point was found to be less than 0.12%. Thus, for a measured pH value of 7.00 obtained from a 25-μm-thick sample, the actual value was expected to be within the range of 6.992–7.008.

pO_2 measurements — Phosphorescence quenching microscopy (PQM). High-resolution PQM was developed for simultaneous use with FRIM. The exponential decay of phosphorescence from albumin-bound palladium *meso*-tetra-(4-carboxyphenyl) porphyrin (Medical Systems Corp., Greenvale, NY) after a pulse excitation is O_2-dependent[45,46]. Immediately after pH measurements, the probe was injected into the tail vein (60 mg/kg). After 30 min, the phosphorescence signal resulting from the 540-nm flashlamp excitation (EG&G, Salem, MA) of the tissue was detected (≥630 nm; Oriel) with a photomultiplier tube (9203B, Products for Research, Danvers, MA) and averaged on a digital oscilloscope (TDS-320, Tektronix, Beaverton, OR) before computer storage (Fig. 1). The excitation field was reduced to a 100-μm diameter spot, using an adjustable diaphragm and the ×40 objective, and a 10 × 10-μm² slit was placed in the emission light path (Fig. 1). This resulted in a depth of light collection of 25 μm, similar to that of pH measurements. Imaging tests showed that light contamination from outside the collecting slit area was minimal (≤8%). A second eyepiece between the slit and the photomultiplier tube (Fig. 1) allowed the viewer to refocus the field of view to the slit before phosphorescence lifetime measurements. Averaging phosphorescence decays after several pulse excitations was necessary to reduce instrumentation noise. However, during a multiple excitation sequence, the porphyrin probe itself may consume a significant amount of oxygen[47]. With our optical configuration, *in vitro* tests with static fluid samples showed that this phenomenon was significant upon >15 excitation flashes and more pronounced at low oxygen tensions (<10 mmHg). Consequently, only five excitation flashes per measurement were used, while an adequate signal-to-noise ratio and a lateral spatial resolution of 10 × 10 μm² were maintained, without any significant transport effects. Phosphorescence decay was not affected by hemoglobin[41], thus measurements were valid both at interstitial and vascular locations.

Calibration was performed as follows. *In vivo* decay signals were first fitted with an exponential function ($r^2 \geq 0.985$). The lifetimes (τ) were then converted to pO_2 values according to the Stern-Volmer equation: $1/\tau = 1/\tau_0 + k_q \times pO_2$, where τ_0 is the phosphorescence lifetime in the absence of oxygen and k_q a quenching constant. Sealed capillary tubes containing static fluid solutions at 40 °C were equilibrated for 30 min with known pO_2 values (3.8, 7.6, 38 and 76 mmHg). A 0-mmHg pO_2 solution was obtained enzymatically using a β-glucose substrate (0.3%) and the glucose oxidase-catalase reactions (glucose oxidase, 75 μg/ml; catalase, 12.5 μg/ml)[46]. An excellent linear fit ($r^2 = 0.998$) between $1/\tau$ and pO_2 (Stern-Volmer equation) was obtained in the pO_2 range of interest (0–38 mmHg), with values of $\tau_0 = 502$ μs and $k_q = 386$ mmHg$^{-1} \cdot s^{-1}$. Because of heterogeneity in tumor pH, calibration was performed at three pH values of 6.60, 7.00 and 7.40. We observed a negligible variation (≤4.0%) in both τ_0 and k_q. Calibration

tests using either collagen type I solutions or culture medium gave similar results.

The feasibility of sequential pH and pO_2 measurements at the same location was assessed both *in vitro* and *in vivo*. pO_2 lifetime values were virtually identical (≤0.2% variation) in the presence or absence of the pH probe. pH fluorescence ratio values, however, were affected by the presence of the porphyrin probe (spectral overlap at the BCECF excitation wavelengths). Therefore, in each experiment, pH measurements preceded pO_2 measurements.

Statistics. Results are presented as means ± s.e.m. Values of several groups were compared by means of the Wilcoxon test for dependent groups, and the Kruskal-Wallis and the Mann-Whitney U-test for independent groups (Statview; Abacus, Berkeley, CA). *P* values smaller than 1% were considered to be significant. The Spearman correlation coefficient, r_s, was calculated to test correlation between parameters. The correlation was considered strong for $r_s > 0.90$, moderate for $0.60 < r_s < 0.65$ and weak for $0.50 < r_s < 0.60$; $r_s < 0.50$ indicated no correlation.

Acknowledgment

This work was supported by an NCI Outstanding Investigator Grant (R35-CA-56591) to R.K.J. M.D. was a recipient of a Feodor-Lynen Fellowship from the Alexander von Humboldt Foundation (1993–1995). We thank M. Intaglietta for his help in setting up the PQM technique, and L.T. Baxter, L.E. Gerweck and H.D. Suit for their critical comments.

RECEIVED 22 AUGUST; ACCEPTED 20 DECEMBER 1996

1. Vaupel, P., Kallinowski, F. & Okunieff, P. Blood flow, oxygen and nutrient supply, and metabolic microenvironment of human tumors: A review. *Cancer Res.* **49**, 6449–6465 (1989).
2. Gullino, P.M., Grantham, F.H., Courtney, A.H. & Losonczy, I. Relationship between oxygen and glucose consumption by transplanted tumors *in vivo*. *Cancer Res.* **27**, 1041–1052 (1967).
3. Casciari, J.J., Sotirchos, S.V. & Sutherland, R.M. Variations in tumor cell growth rates and metabolism with oxygen concentration, glucose concentration, and extracellular pH. *J. Cell. Physiol.* **151**, 386–394 (1992).
4. Engin, K. *et al.* Extracellular pH distribution in human tumours. *Int. J. Hyperthermia* **11**, 211–216 (1995).
5. Shweiki, D., Itin, A., Soffer, D. & Keshet, E. Vascular endothelial growth factor induced by hypoxia may mediate hypoxia-initiated angiogenesis. *Nature* **359**, 843–845 (1992).
6. Shimizu, S. *et al.* Induction of apoptosis as well as necrosis by hypoxia and predominant prevention of apoptosis by Bcl-2 and Bcl-X_L. *Cancer Res.* **56**, 2161–2166 (1996).
7. Graeber, T.G. *et al.* Hypoxia-mediated selection of cells with diminished apoptotic potential in solid tumours. *Nature* **379**, 88–91 (1996).
8. Young, P.R. & Spevacek, S.M. Substratum acidification by murine B16F10 melanoma cultures. *Biochim. Biophys. Acta* **1139**, 163–166 (1992).
9. Turner, G.A. Increased release of tumor cells by collagenase at acid pH: A possible mechanism for metastasis. *Experientia* **35**, 1657–1658 (1979).
10. Krtolica, A. & Ludlow, J.W. Hypoxia arrests ovarian carcinoma cell cycle progression, but invasion is unaffected. *Cancer Res.* **56**, 1168–1173 (1996).
11. Loeffler, D.A., Juneau, P.L. & Masserant, S. Influence of tumour physico–chemical conditions on interleukin-2-stimulated lymphocyte proliferation. *Br. J. Cancer* **66**, 619–622 (1992).
12. Suit, H. Tumor oxygenation and radiosensitivity. in *Blood Substitutes: Physiological Basis of Efficacy* (eds. Winslow, R.M. *et al.*) 187–199 (Birkhäuser, Boston, 1995).
13. Wike-Hooley, J.L., Haveman, J. & Rheinhold, H.S. The relevance of tumor pH to the treatment of malignant disease. *Radiother. Oncol.* **2**, 343–366 (1984).
14. Tannock, I.F. & Rotin, D. Acid pH in tumors and its potential for therapeutic exploitation. *Cancer Res.* **49**, 4373–4384 (1989).
15. Song, C.W., Lyons, J.C. & Luo, Y. Intra- and extracellular pH in solid tumors: Influence on therapeutic response. in *Drug Resistance in Oncology* (ed. Teicher, B.A.) 25-51 (Marcel Dekker, New York, 1993).
16. Ward, K.A. & Jain, R.K. Response of tumours to hyperglycaemia: Characterization, significance and role in hyperthermia. *Int. J. Hyperthermia* **4**, 223–50 (1988).
17. Griffiths, J.R. Are cancer cells acidic? *Br. J. Cancer* **64**, 425–427 (1991).
18. Jain, R.K., Shah, S.A. & Finney, P.L. Continuous noninvasive monitoring of pH and temperature in rat Walker 256 carcinoma during normoglycemia and hyperglycemia. *J. Natl. Cancer Inst.* **73**, 429–36 (1984).
19. Gray, L.H., Conger, A.S.D., Ebert, M., Hornsey, S. & Scott, O.C.A. The concentration of oxygen dissolved in tissue at the time of irradiation as a factor in radiotherapy. *Br. J. Radiol.* **26**, 638–648 (1953).
20. Chaplin, D.J. & Acker, B. The effect of hydralazine on the tumor cytotoxicity of the hypoxic cell cytotoxin RSU 1069: Evidence for therapeutic gain. *Int. J. Radiat. Oncol. Biol. Phys.* **13**, 579–586 (1987).
21. Skarsgard, L.D., Skwarchuk, M.W., Vinczan, A., Kristl, J. & Chaplin, D.J. The cytotoxicity of melphalan and its relationship to pH, hypoxia and drug uptake. *Anticancer Res.* **15**, 219–224 (1995).
22. Teicher, B.A., Lazo, J.S. & Sartorelli, A.C. Classification of antineoplastic agents by their selective toxicities towards oxygenated and hypoxic tumor cells. *Cancer Res.* **41**, 73–81 (1981).
23. Jähde, E. *et al.* Hydrogen ion-mediated enhancement of cytotoxicity of bischloroethylating drugs in rat mammary carcinoma cells in vitro. *Cancer Res.* **49**, 2965–2972 (1989).
24. Karuri, A.R., Dobrowsky, E. & Tannock, I.F. Selective acidification and toxicity of weak organic acids in an acidic microenvironment. *Br. J. Cancer* **68**, 1080–1087 (1993).
25. Gerweck, L.E. & Seetharaman, K. Cellular pH gradient in tumor versus normal tissue: Potential exploitation for the treatment of cancer. *Cancer Res.* **56**, 1194–1198 (1996).
26. Hoeckel, M. *et al.* Intratumoral pO_2 predicts survival in advanced cancer of the uterine cervix. *Radiother. Oncol.* **26**, 45–50 (1993).
27. Engin, K., Leeper, D.B., Thistlethwaite, A.J., Tupchong, L. & McFarlane, J.D. Tumor extracellular pH as a prognostic factor in thermoradiotherapy. *Int. J. Radiat. Oncol. Biol. Phys.* **29**, 125–132 (1994).
28. Schwickert, G., Walenta, S., Sundfør, K., Rofstad, E.K. & Mueller-Klieser, W. Correlation of high lactate levels in human cervical cancer with incidence of metastasis. *Cancer Res.* **55**, 4757–4759 (1995).
29. Brizel, D.M. *et al.* Tumor oxygenation predicts for the likelihood of distant metastases in human soft tissue sarcoma. *Cancer Res.* **56**, 941–943 (1996).
30. Vaupel, P.W., Frinak, S. & Bicher, H.I. Heterogeneous oxygen partial pressure and pH distribution in C3H mouse mammary adenocarcinoma. *Cancer Res.* **41**, 2008–2013 (1981).
31. Daly, P.F. & Cohen, J.S. Magnetic resonance spectroscopy of tumors and potential in vivo clinical applications: A review. *Cancer Res.* **49**, 770–779 (1989).
32. Hawkins, R.A. & Phelps, M.E. PET in clinical oncology. *Cancer Metastasis Rev.* **7**, 119–142 (1988).
33. Evans, S.M., Jenkins, W.T., Joiner, B., Lord, E.M. & Koch, C.J. 2-Nitroimidazole (EF5) binding predicts radiation resistance in individual 9L s.c. tumors. *Cancer Res.* **56**, 405–411 (1996).
34. Gullino, P.M., Clark, S.H. & Grantham, F.H. The interstitial fluid of solid tumors. *Cancer Res.* **24**, 780–797 (1964).
35. Jain, R.K. Delivery of molecular medicine to solid tumors. *Science* **271**, 1079–1080 (1996).
36. Warburg, O. *The Metabolism of Tumors* (R.R. Smith, New York, 1931).
37. Acker, H., Carlsson, J., Holtermann, G., Nederman, T. & Nylén, T. Influence of glucose and buffer capacity in the culture medium on growth and pH in spheroids of human thyroid carcinoma and human glioma origin. *Cancer Res.* **47**, 3504–3508 (1987).
38. Sutherland, R.M. *et al.* Oxygenation and differentiation in multicellular spheroids of human colon carcinoma. *Cancer Res.* **46**, 5320–5329 (1986).
39. Casciari, J.J., Sotirchos, S.V. & Sutherland, R.M. Glucose diffusivity in multicellular tumor spheroids. *Cancer Res.* **48**, 3905–3909 (1988).
40. Dewhirst, M.W. *et al.* Perivascular oxygen tensions in a transplantable mammary tumor growing in a dorsal flap window chamber. *Radiat. Res.* **130**, 171–182 (1992).
41. Torres-Filho, I.P., Leunig, M., Yuan, F., Intaglietta, M. & Jain, R.K. Noninvasive measurement of microvascular and interstitial oxygen profiles in a human tumor in SCID mice. *Proc. Natl. Acad. Sci. USA* **91**, 2081–5 (1994).
42. Martin, G.R. & Jain, R.K. Noninvasive measurement of interstitial pH profiles in normal and neoplastic tissue using fluorescence ratio imaging microscopy. *Cancer Res.* **54**, 5670–5674 (1994).
43. Dellian, M., Helmlinger, G., Yuan, F. & Jain, R.K. Interstitial pH in solid tumours measured by fluorescence ratio imaging and optical sectioning: Effect of glucose on spatial and temporal gradients. *Br. J. Cancer* **74**, 1206–1215 (1996).
44. Leunig, M. *et al.* Angiogenesis, microvascular architecture, microhemodynamics, and interstitial fluid pressure during early growth of human adenocarcinoma LS174T in SCID mice. *Cancer Res* **52**, 6553–60 (1992).
45. Torres Filho, I.P. & Intaglietta, M. Microvessel pO_2 measurements by phosphorescence decay method. *Am. J. Physiol.* **265**, H1434–H1438 (1993).
46. Vanderkooi, J.M., Maniara, G., Green, T.J. & Wilson, D.F. An optical method for measurement of dioxygen concentration based upon quenching of phosphorescence. *J. Biol. Chem.* **262**, 5476–5482 (1987).
47. Zheng, L., Golub, A.S. & Pittman, R.N. Determination of pO_2 and its heterogeneity in single capillaries. *Am. J. Physiol.* **271**, H365–H372 (1996).